Collection Efficiency for Filters with Staggered Parallel Y and Triple Y Fibers: A Numerical Study

Huaning Zhu, Juan P. Hinestroza

College of Human Ecology, Cornell University, Ithaca, New York, USA

Correspondence to:
Juan P. Hinestroza, email: jh433@cornell.edu

ABSTRACT

A numerical study is performed to determine the collection efficiency of filters composed of staggered parallel Y and triple Y fibers. By employing the Lattice Boltzmann method, the Navier–Stokes equations are solved for flow fields in a two-dimensional domain with periodic boundary conditions. Trajectories of particles with different diameters arranging from 0.02 μm to 5 μm are then computed by solving the particle motion equation hence obtaining the collection efficiency of single Y and triple Y fibers. The effects of fiber orientation, Brownian motion, particulate size and Reynolds number on the collection efficiency of these two types of fibers are also evaluated numerically.

Y and triple Y fibers have low packing density and relatively large area to volume ratio, and the latter property helps enhance the Brownian diffusion collection mechanism for smaller particles. The large void zone of these fibers can accommodate more particles, which improves the particle loading capacity. It is also found out that the flow field and collection efficiency of triple Y fiber is less susceptible to different fiber orientations due to its geometric symmetry. The numerical results obtained in this work provide helpful information in designing high efficiency filters.

INTRODUCTION

Fibrous filters have been widely used to remove particles from a gas flow. The effectiveness of filters in capturing particles is mainly achieved through the combined effect of Brownian diffusion, interception, inertial impaction and gravitational sedimentation. Electrostatics may also affect fibrous filtration depending on particle size and electro-properties of the filter material. Conventional fibrous filters are made of randomly packed long cylindrical fibers, however, fibers with noncircular cross-section have great potential to make filters with possible enhancement in porosity, particle loading capacity and collection efficiency. As a result, research in fibrous media shows a growing interest in fibers with noncircular cross-sections in the past decades [1-7]. For example, Fardi and Liu [1-2] developed a numerical model for solving the flow field through a staggered array of rectangular fibers, and then determined the single-fiber collection efficiency due to the mechanical collection mechanisms (inertial impaction, interception and diffusion). Based on Fardi and Liu's approach [1-2], Chen et al. conducted a numerical study to determine the collection efficiency of a single rectangular fiber under different fiber aspect ratio, filter packing density, particulate size and Reynolds [5]. Zhu et al. investigated the impaction-dominated filtration process for filters with rectangular fibers [6]. By considering the electrostatic force, Cao et al. also developed a numerical model to simulate the collection efficiency of singly charged or neutral particles in an electret filter composed of array of rectangular fibers [7].

Considering that Y and triple Y fibers have large porosity, large surface area to volume ratio, and large particle loading capacity, we investigated the collection efficiency of filters consisting of staggered array of parallel Y or triple Y fibers. We first computed the flow field in a representative cell containing a single or triple Y fiber. To handle the complex geometry and boundary conditions of the flow problem we choose to use the Lattice Boltzmann method (LBM), which has been established as a powerful alternative to the conventional Navier-Stokes solvers in computational fluid dynamics [8-11]. The LBM provides numerous advantages, including clear physical pictures, multi-scale simulation capabilities, and fully parallel algorithms. In addition, complex boundary conditions can be implemented in LBM easily through a so-called "bounce-back" scheme. After the flow field is obtained, trajectories of particles with different diameters arranging from 0.02 μm to 5 μm were computed by solving the particle motion equation in order to obtain the collection efficiency of single Y and triple Y fibers. A detailed analysis of the numerical results is presented in the results and discussions section, which helps understand the effect

of fiber orientation, Brownian motion, particulate size and Reynolds number on the collection efficiency of these two types of non-circular fibers.

THEORY

Computation of Flow Field using Lattice Boltzmann Method

In the Lattice Boltzmann method, the fluid is represented by particles with discrete velocities. The interaction between the particles is described by a linearized relaxation-type collision term. The Navier–Stokes equations follow from this model as a low-Mach number limit and the viscosity of the liquid linearly depends on the relaxation rate. Among the Lattice Boltzmann methods reported in the literature, the most widely used one is the lattice Boltzmann Bhatnagar-Gross-Krook (BGK) model, which is abbreviated as LBGK [8, 10]. The LBGK equation utilizes a single relaxation time approximation and is described by the following equation,

$$f_i\left(x+\mathbf{c}_i\delta t, t+\delta t\right)-f_i\left(x,t\right) = -\frac{1}{\tau}\left[f_i\left(x,t\right)-f_i^{eq}\left(x,t\right)\right], \quad i=0,\,1,\ldots q-1, \tag{1}$$

where $f_i(x,t)$ is the density distribution function along the i direction at lattice site x and time t, δt is the time step, $\mathbf{c}_i$ is the discrete velocity and τ is the dimensionless single-relaxation time. Function f_i^{eq} is the local Maxwell type distribution function expressed as a Taylor expansion to second-order in fluid velocity. The density ρ and bulk velocity $\boldsymbol{u}$ can be determined from

$$\rho=\sum_{i=0}^{q-1} f_i\,, \tag{2}$$

$$\rho\,\mathbf{u}=\sum_{i=0}^{q-1}\mathbf{c}_i\,f_i\,, \tag{3}$$

respectively. The relaxation time τ can be related to the kinematic viscosity v by

$$\nu=c_s^2\,\delta t\left(\tau-0.5\right), \tag{4}$$

for a square lattice, where c_s is the sound speed of the lattice fluid, which is defined as $c_s^2=1/3$.

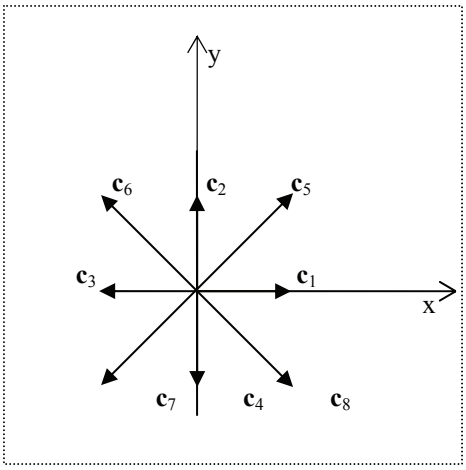

FIGURE 1: Schematic plot of particle velocity for the D2Q9 model. An additional vector with zero components $\mathbf{c}_0 = (0, 0)$ is defined denoting a rest particle population.

In the popular nine-velocity square lattice model D2Q9, the particle velocities, $\mathbf{c}_i$, are given by Qian *et al*. [11]

$$\begin{aligned}
&\mathbf{c}_0 = 0,\\
&\mathbf{c}_i = \left[cos\left((i-1)\pi/2\right), sin\left((i-1)\pi/2\right)\right],\\
&\quad i=1-4,\\
&\mathbf{c}_i = \sqrt{2}\left[cos\left((i-5)\pi/2+\pi/4\right), sin\left((i-5)\pi/2+\pi/4\right)\right],\\
&\quad i=5-8.
\end{aligned} \tag{5}$$

The equilibrium distribution for the D2Q9 model as stated by Qian *et al*. is: [11]

$$\begin{aligned}
&f_i^{eq}=\rho\,\omega_i\left[1+3\mathbf{c}_i\cdot\mathbf{u}+\frac{9}{2}\left(\mathbf{c}_i\cdot\mathbf{u}\right)^2-\frac{3}{2}\mathbf{u}\cdot\mathbf{u}\right],\\
&\omega_0=\frac{4}{9},\ \omega_i=\frac{1}{9},\ i=1-4,\quad \omega_i=\frac{1}{36},\ i=5-8.
\end{aligned} \tag{6}$$

Through a multi-scale Chapman-Enskog analysis of the LBGK model [8,10], it can be shown that the macroscopic variables ρ and $\boldsymbol{u}$ defined in equations (2) and (3) obey the Navier–Stokes equation for a weakly compressible fluid

$$\partial_t\rho+\nabla\cdot\left(\rho\,\mathbf{u}\right)=0\,, \tag{7}$$

$$\partial_t\mathbf{u}+\left(\mathbf{u}\cdot\nabla\right)\mathbf{u}=-\frac{1}{\rho}\nabla\,p+\nu\,\nabla^2\mathbf{u}\ . \tag{8}$$

And the pressure is given by the equation of state

$$p = c_s^2 \rho \,. \tag{9}$$

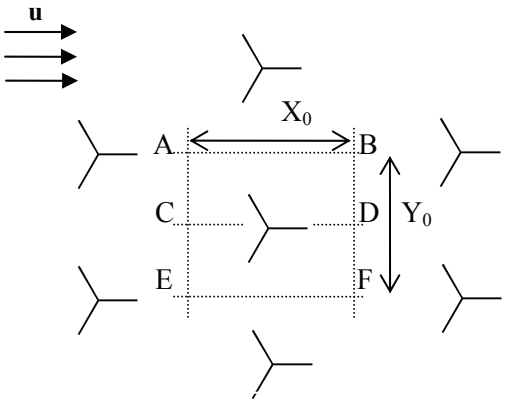

FIGURE 2: Geometry of staggered array of Y fibers

The filter is modeled as a staggered array of infinitely long parallel Y or triple Y fibers, facing to a horizontal flow direction, as shown in *Figure 2*. The flow field is assumed to develop a periodic pattern along the flow direction therefore it can be computed using to a representative cell ABEF. In the actual computations we employ only half of the original cell by taking advantage of the symmetry property of this flow field where the upper part ABCD is an inversion of the other half CDEF.

The collection efficiency is computed under a steady flow field and the Buoyancy effects are neglected. A no-slip boundary condition is applied at the interface between fluid and fiber. Following Chen et al. [5], the boundary conditions for the computation domain ABCD are expressed as follows:

along the upper boundary AB

$$\partial_y u_x = 0,\ u_y = 0\,, \tag{10}$$

along the lower boundary CD

$$\partial_y u_x = 0,\ u_y = 0\,, \tag{11}$$

along the surface of the fiber

$$u_x = 0,\ u_y = 0\,, \tag{12}$$

and long the left boundary AC,

$$\begin{aligned} u_x(x,y) &= u_x(x + X_0, Y_0/2 - y), \\ u_y(x,y) &= -u_y(x + X_0, Y_0/2 - y). \end{aligned} \tag{13}$$

Collection Efficiency of a Single Fiber

A rigorous analysis of the two-way coupling of particle and fluid interactions is needed for a complete understanding of particulate flows around fibers [12]. However, for engineering applications of very dilute particulate suspensions, with particle volume concentrations less than 0.1%, the effect of particles on the flow field may become negligible [6]. Under such conditions the fluid and solid phases can be treated separately. In the absence of external forces such as electrostatic and gravitational forces the trajectory of individual particles can be determined by solving the following equations of particle motion:

$$\frac{d\mathbf{u}}{dt} = \mathbf{a}_d + \mathbf{a}_{\mathrm{r}} \tag{14}$$

$$\mathbf{a}_d = \frac{18\mu}{\rho_p d_p^2 C_c}\left(\mathbf{u} - \mathbf{u}_p\right) \tag{15}$$

where $\mathbf{u}_p$ is particle velocity, ρ_p and d_p are the density and diameter of particles, respectively. The term $\mathbf{a}_d$ in equation (14) is the acceleration of a particle due to the drag force, in which the relative slip between the particle and the fluid is also considered. Variable *Cc* is the Stokes–Cunningham slip factor given by Abuzeid et al. [13]

$$C_c = 1 + \frac{2\lambda}{d_p}\left(1.257 + 0.4\, e^{-1.1 d_p / 2\lambda}\right) \tag{16}$$

where λ is the mean free path of the gas phase. The term $\mathbf{a}_r$ in equation (14) is acceleration due to the Brownian diffusion effects, which plays an important role for submicron particles. Following Abuzeid et al. [13], Chen et al. [5] and Cao et al. [6], the Brownian force is modeled as a Gaussian random process. The component of the Brownian force for unit mass, $\mathrm{a}_{\mathrm{r}}^{\mathrm{i}}\,(i = x, y)$ at any time step *t* is calculated as

$$\mathrm{a}_{\mathrm{r}}^{\mathrm{i}}(t) = Z_i \sqrt{\frac{2\pi S_0}{\Delta t}} \tag{17}$$

where Z_i is a random number with a zero mean and unit variance, while Δt is the time step. The term S_0

is the spectral intensity of a white noise process [14-15], given by

$$S_0 = \frac{216\mu kT}{\pi^2 d_p^5 \rho_p^2 C_c} \tag{18}$$

where T is the fluid absolute temperature and k is the Boltzmann constant.

A large number of particles are required for statistical reliability of the computational results. Positions of the approaching particles on the inlet plane are randomly chosen [5, 7], and for each particle the trajectory is obtained by numerically integrating equation (14). The number of particles which are collected by the fiber or leave the computation cell is counted. The collection efficiency of particles for a single fiber is consequently defined as the ratio of the number of particles collected on the fiber to the number of particles entering the computational domain.

RESULTS AND DISCUSSIONS

In the present study, the size of the representative cell (ABEF in *Figures* 2) is 200μm times 200μm and within the cell Y or triple Y fibers are situated in the center.

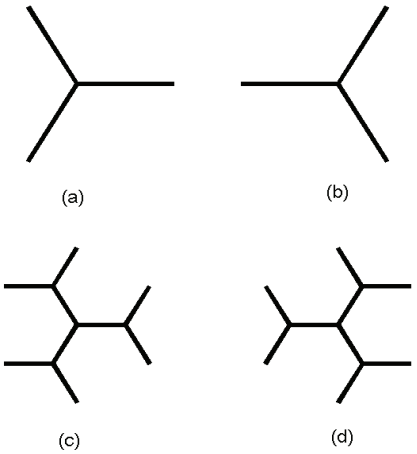

FIGURE 3: Illustration of geometry of Y and triple Y fibers: (a) Y fiber (b) Y fiber in reversed orientation (c) triple Y fiber and (d) triple Y fiber in reversed orientation.

For each Y or triple Y fiber we also consider its reversed orientation; therefore there are totally four types of geometry configurations, Y fiber and Y fiber with reversed orientation, triple Y fiber and triple Y fiber with reversed orientation (*Figures* 3a-d). The Y fiber is composed of three equal length (33.3μm) branches which join at the center of the domain. The width of these fiber branches is 4μm and the angles these branches make with positive x-axis are 0, 120 and 240 degree, respectively. As for the Y fiber with reversed orientation the angles these three branches make with the positive x-axis are 60, 180 and 300 degree, respectively. The triple Y fibers consist of three smaller size Y fibers that join at the center of the domain (*Figures* 3c). The length of the branches of the smaller Y fibers is 16.7μm. Triple Y fiber with reversed orientation is also considered (*Figures* 3d). It is noted that all these four fibers have the same interception ratio 28.9% perpendicular to the flow direction, i.e. positive x direction.

The fiber volumetric packing density is 1.0% for the Y fibers and 1.5% for the triple Y fibers. Particle density chosen is 2000 kg/m^3 and the gas viscosity is 1.79 10^5 kg/m s. Two Reynolds numbers 1 and 10 of the flow fields are considered in the present study, which are computed based on the length of the representative cell.

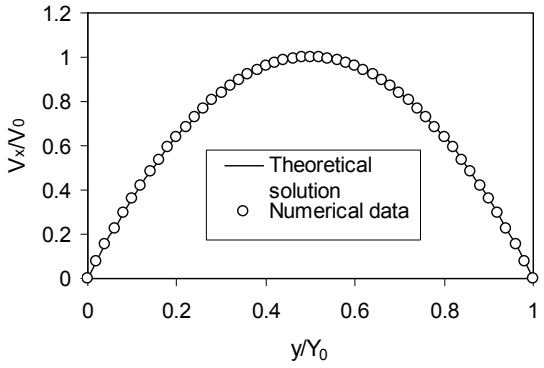

FIGURE 4: Velocity profiles of plane Poiseuille flow.

As a verification of our LBM algorithm, we first performed a numerical simulation of a standard plane Poiseuille flow and compare numerical results with analytical solutions. *Figure 4* shows a good quantitative agreement between the numerical results and the analytical solution.

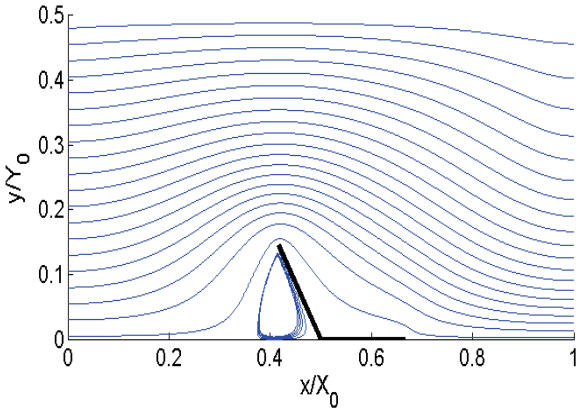

FIGURE 5a: Streamline around a Y fiber, Re =1

To obtain a reliable flow field, a convergence test is performed by refining lattice densities until a 1% tolerance for velocity is reached. The discrete lattice employed for the computational cell ABCD was 200 by 100 in x and y direction, respectively.

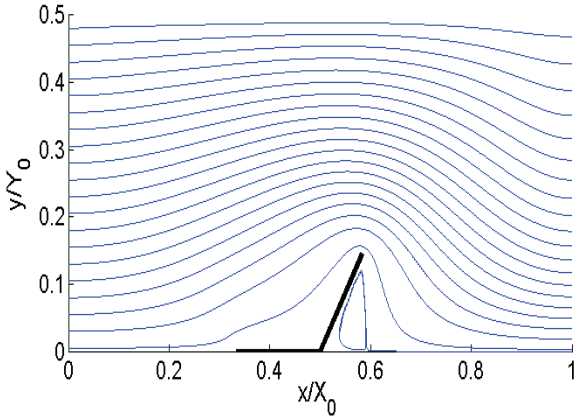

FIGURE 5b: Streamline around a Y fiber in reversed orientation, Re =1.

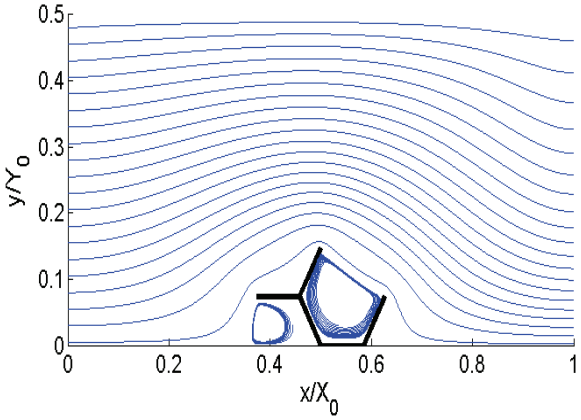

FIGURE 5c: Streamline around a triple Y fiber, Re =1.

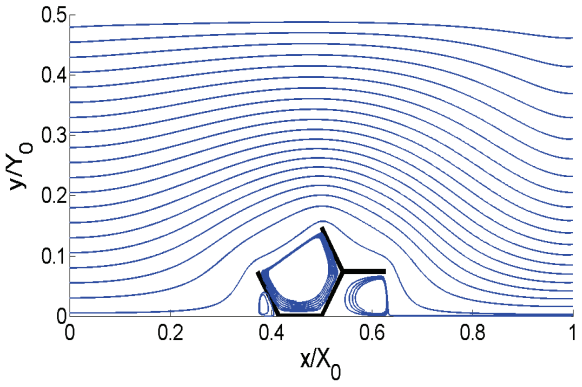

FIGURE 5d: Streamline around a triple Y fiber in reversed orientation, Re =1.

Figures 5a-d show the streamlines for Y and triple Y fibers with different orientations. The re-circulation zones can be found at different locations depending on the fiber geometry and flow direction. It is also observed that the two flow patterns for the flow domains containing triple Y fibers (*Figures 5c-5d*) are closer than those in the domain containing Y fibers (*Figure. 5a-5b*). This is mainly due to the fact that the six end points of the outer branches of the triple Y fiber have the same space coordinates as those of the triple Y fiber with reversed orientation. In other words the triple Y fibers have a more isotropic geometry configuration, which has an impact on the corresponding flow field.

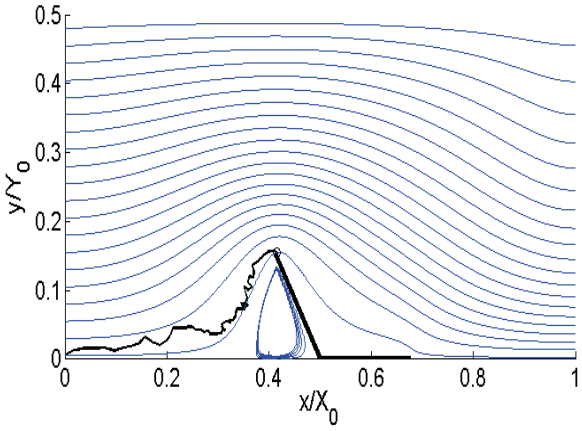

FIGURE 6a: Particle trajectory, $d_p = 0.02\,\mu m$, Re =1.

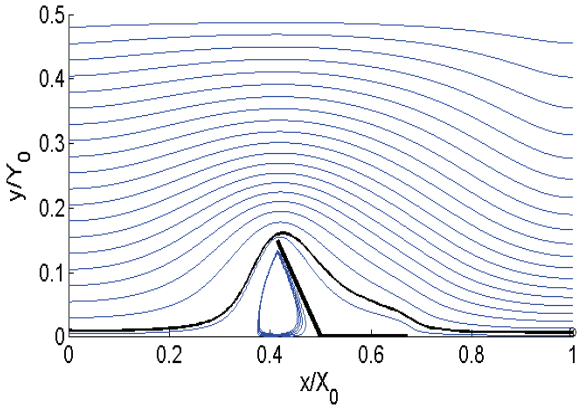

FIGURE 6b: Particle trajectory, $d_p = 1\,\mu m$, Re =1.

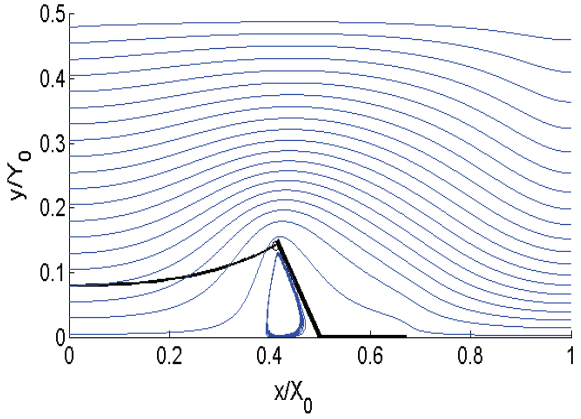

FIGURE 6c: Particle trajectory, $d_p = 5\,\mu m$, Re =10.

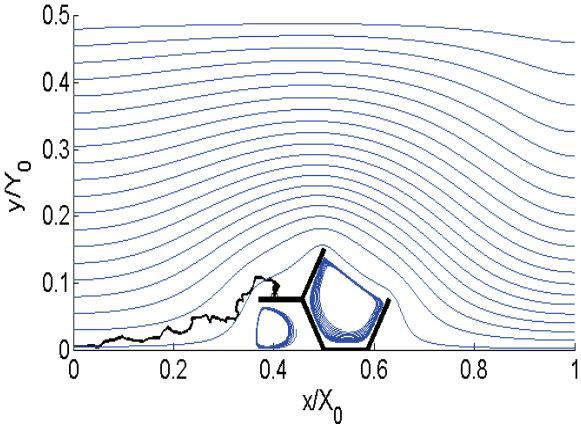

FIGURE 6d: Particle trajectory, $d_p = 0.02\,\mu m$, Re =1.

Figures 6a to *6d* show the trajectories of particles with different sizes, which consider Brownian diffusion. Specifically, *Figure 6a* shows the trajectory of a particle with $d_p = 0.02\,\mu m$ under the flow condition of Re = 1. The zigzag path of the particle trajectory illustrates the dominant Brownian diffusion effects. For a particle of $d_p = 1\,\mu m$ under the same Reynolds number Re = 1 (*Figure 6b*), the Brownian motion effects becomes less important and the particle trajectory approximately follows the streamline. Under such circumstances, the main collection mechanism becomes interception. As the particle size increases and Reynolds number becomes larger, the particle trajectories deviate the streamline and the major collection mechanism becomes inertial impaction. *Figure 6c* shows the inertial impaction effect for a particle with $d_p = 5\,\mu m$ under the flow of Re =10. *Figure 6d* illustrates the effect of Brownian motion.

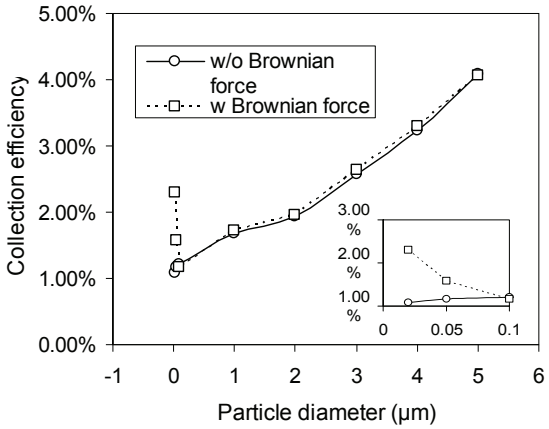

FIGURE 7a: Collection efficiency of a Y fiber for particles with different diameters, Re =1.

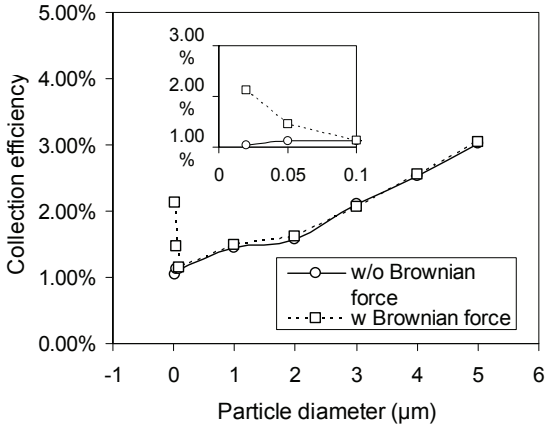

FIGURE 7b: Collection efficiency of a Y fiber with reversed orientation for particles with different diameters, Re =1.

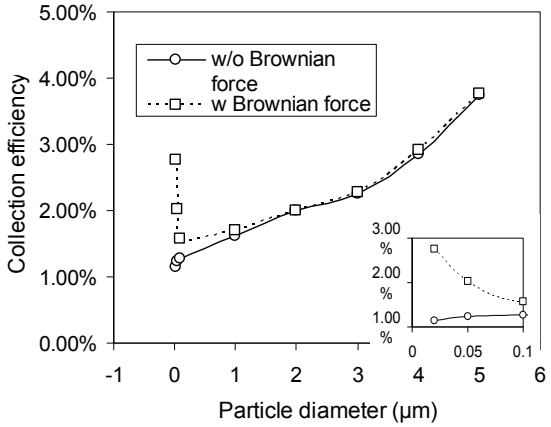

FIGURE 7c: Collection efficiency of a triple Y fiber for particles with different diameters, Re =1.

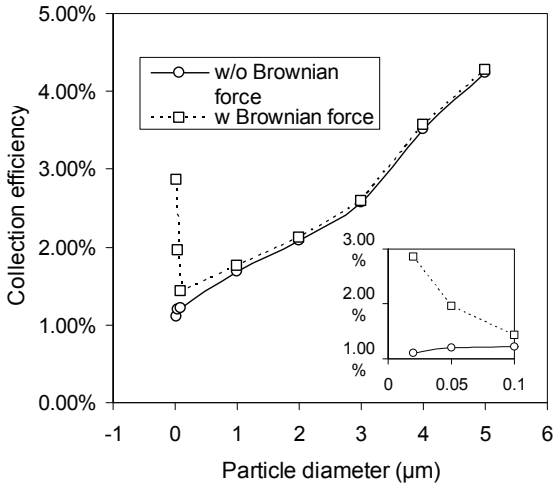

FIGURE 7d: Collection efficiency of a triple Y fiber with reversed orientation for particles with different diameters, Re =1.

Figures 7a-d show the simulated single fiber collection efficiencies for particles with size ranging from 0.02 μm to 5 μm under the flow field of Re =1. Without Brownian diffusion effects, the collection efficiency is a monotonically increasing function of particle size; while considering Brownian effects, the collection efficiency first decreases as particle size increases until minimum value is reached and then increases with further increases in particle size. It is found that the values of collection efficiency are significantly higher for particles smaller than 0.1μm when the Brownian diffusion effect of particles is a dominant collection mechanism. As the particle size becomes larger than 1μm, the inertial impaction collection becomes more important resulting in higher collection efficiency.

By comparing the collection efficiency between the Y and triple Y fibers, we also find that for smaller particles the collection efficiency values of the triple Y fibers are higher than those of Y fibers. Obviously, the larger surface area of triple Y fibers is in favor of Brownian diffusion effect.

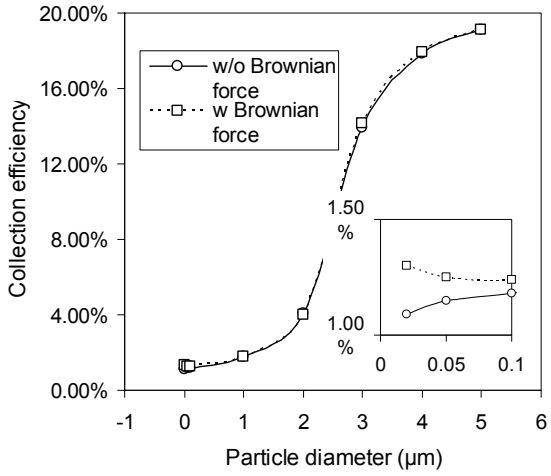

FIGURE 8a: Collection efficiency of a Y fiber for particles with different diameters, Re =10.

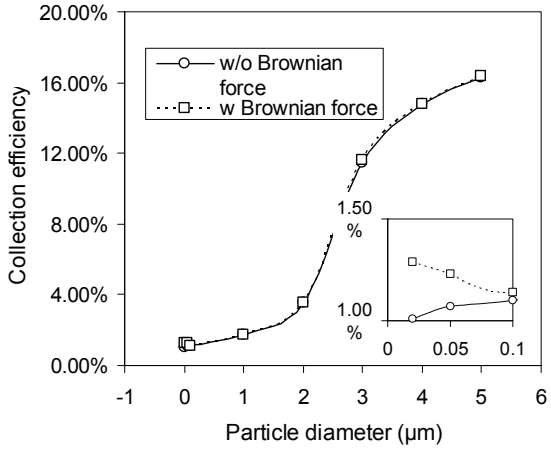

FIGURE 8b: Collection efficiency of a Y fiber with reversed orientation for particles with different diameters, Re =10.

Figures 8a-d show the single fiber collection efficiencies for different size of particles under the flow field of Re =10. As the particle size increases, the collection efficiency increases significantly, because at high Reynolds number and large particle size the inertial impaction dominates the other mechanisms. It is also noticed that at a higher Reynolds number of Re =10, the Brownian diffusion

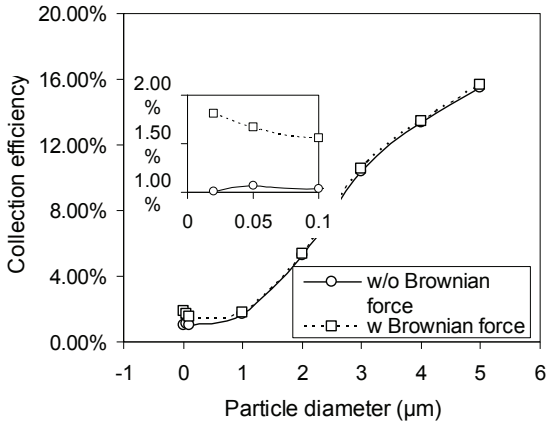

FIGURE 8c: Collection efficiency of a triple Y fiber for particles with different diameters, Re =10.

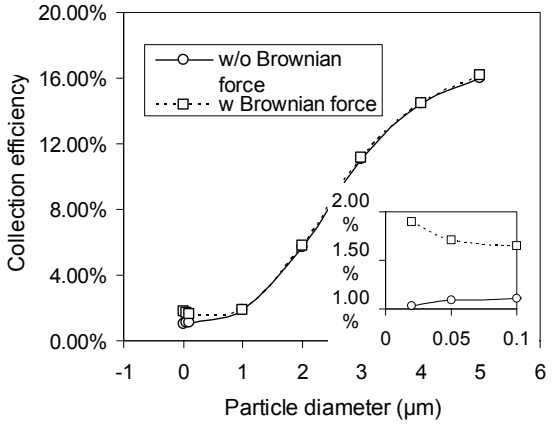

FIGURE 8d: Collection efficiency of a triple Y fiber with reversed orientation for particles with different diameters, Re =10.

effect on collection efficiency is less prominent. As a result, the collection efficiency decreases at higher Reynolds number for smaller particles, which is in accordance with the results of Chen et al. [5] and Ramarao et al. [16] For large particles ($d_p \geq 2\,\mu m$), the collection efficiencies are much higher than those under smaller Reynolds number, a consequence of the domination of inertial impaction mechanism.

Though at higher Reynolds number the Brownian diffusion effect on collection efficiency is less prominent, we can still observe that for smaller particles, the collection efficiency of triple Y fibers is noticeably higher for the cases considering Brownian effects. This difference can hardly be observed for Y fibers. Again, this can be ascribed to the larger surface area of triple Y fibers compared with that of Y fibers.

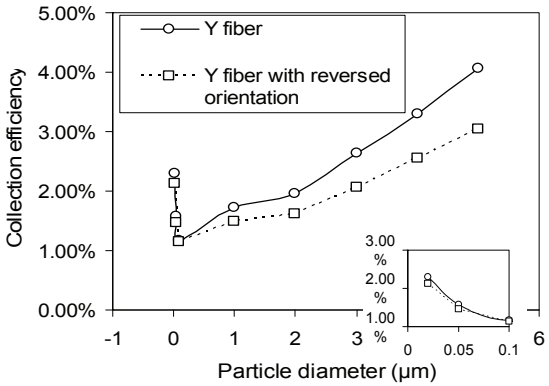

FIGURE 9a: Comparison of collection efficiency of Y fibers with different orientations, Re =1.

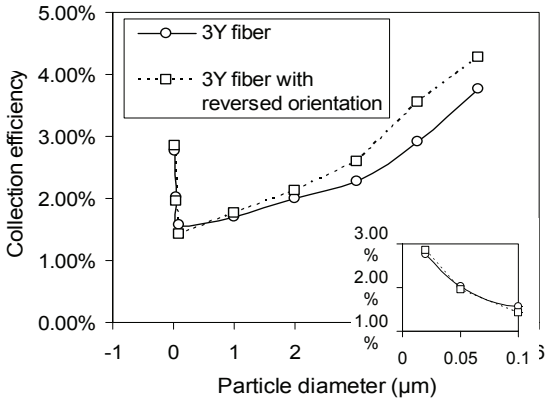

FIGURE 9b: Comparison of collection efficiency of triple Y fibers with different orientations, Re =1.

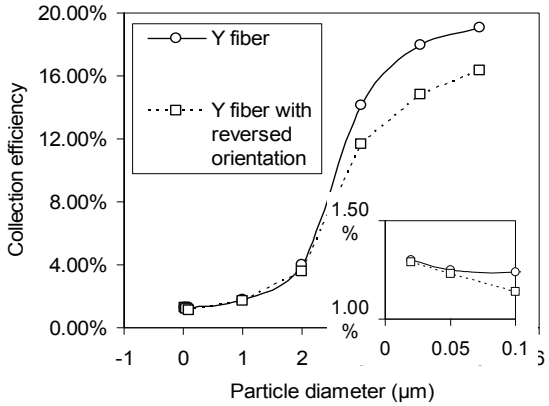

FIGURE 9c: Comparison of collection efficiency of Y fibers with different orientations, Re =10.

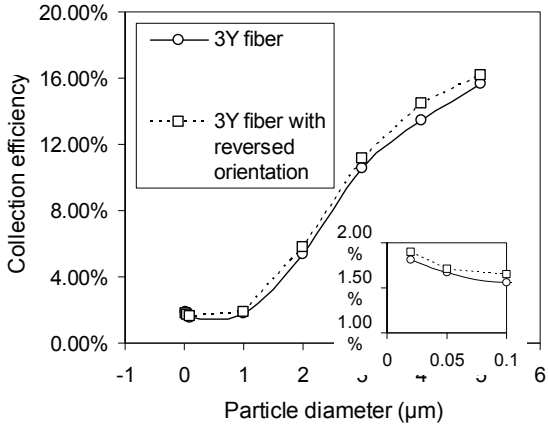

FIGURE 9d: Comparison of collection efficiency of triple Y fibers with different orientations, $\mathrm{Re}=10$.

The comparisons of collection efficiency of Y and triple Y fibers with different orientations and Reynolds numbers are shown in *Figures 9a-d*. The collection efficiency for Y fiber is higher than that of Y fiber with reversed orientation; while for triple Y fibers it is true the other way around. In addition, for flow fields with the same Reynolds number the differences of collection efficiency values between the two triple Y fibers are smaller than that of the two Y fibers. As we have discussed earlier in this section, triple Y fibers have a more isotropic geometry configuration than that of Y fibers, which results in closer flow fields and hence collection efficiency values.

CONCLUSIONS

Collection efficiency of micro and sub-micron sized particles flow through filters consisting of staggered array of Y and triple Y fibers was investigated by considering Brownian diffusion, interception and inertial compaction. The effect of Reynolds number and fiber orientation was also studied.

It is concluded that at low Reynolds numbers, the Brownian diffusion play a major role on collection efficiency, especially for particles with diameter smaller than 0.1 μm. The simulation results also confirm that particle size ranging from 0.1 to 1 μm are harder to capture, in other words, particles in these ranges penetrate the filter most. Other collection mechanisms such as electrostatics might have to be considered in collecting particles in this range. If the particle diameter further increases larger collection efficiency can be achieved, especially under higher Reynolds numbers where inertial impact becomes the dominant mechanism.

The above conclusions are also generally true for aerosol filters with other type of fibers such as rectangular or circular cross-section in shape. What is new for the Y and triple Y fibers in the present study is that they have lower packing density, large area to volume ratio and large void volume. On one hand this increase collection efficiency for smaller particles when Brownian forces dominate; on the other hand those void zones can accommodate more particles, which will potentially extend the service life of these filters. In addition, we fond out that the flow field and collection efficiency of triple Y fibers are less sensitive to fiber orientations due to their geometry symmetry configuration. This is an amenable property in that no matter what direction the air flow through the filter, we are able to achieve similar collection efficiency.

ACKNOWLEDGMENT

This work made use of the Research Computing facility of the Cornell Center for Materials Research (CCMR) with support from the National Science Foundation Materials Research Science and Engineering Centers (MRSEC) program (DMR 0520404).

REFERENCES

[1] Fardi, B., Liu, B. Y. H.; Flow field and pressure drop of filters with rectangular fibers. *Aerosol Science and Technology* 1992, *17*, 36–44.

[2] Fardi, B., Liu, B. Y. H.; Efficiency of fibrous filters with rectangular fibers. *Aerosol Science and Technology* 1992, *17*, 45–58

[3] Ushe, Z.; in: Leung W. W. Ed.., *Advances in Filtration and Separation Technology* 1993, *7*, 146.

[4] Ming O, Y.; Liu B. Y. H.; Analytical solution of flow field and pressure drop for filters with rectangular fibers. *J. Aerosol Science* 1998, *29*, 187–196.

[5] Chen, S., Cheung, C. S., Chan, C. K.; Zhu, C.; Numerical Simulation of Aerosol Collection in Filters with Staggered Parallel Rectangular Fibers, *Computational Mechanics,* 2002, *28,*152–161.

[6] Zhu, C.; Lin, C. H.; Cheung C. S.; Inertial impaction dominated fibrous filtration with rectangular or cylindrical fibers. *Powder Technology,* 2000, *112*,149–162

[7] Cao, Y. H.; Cheung, C. S.; Yan, Z. D.; Numerical Study of an Electret Filter

Composed of an Array of Staggered Parallel Rectangular Split-Type Fibers, *Aerosol Science and Technology*, 2004, *38*, 603–618.

[8] Chen, S.; Doolen, G. D.; Lattice Boltzmann method for fluid flow, *Ann. Rev. Fluid Mech*. 1998, *30*, 329-364.

[9] Lallemand, P.; Luo, L.-S.; Theory of the lattice-Boltzmann method: dispersion, dissipation, isotropy, Galilean invariance, and stability, *Phys. Rev. E,* 2000, *361* 6546–6562.

[10] Chen, S.; Chen, H.; Martinez, D.; Matthaeus, W.; Lattice Boltzmann model for simulation of magnetohydrodynamics, *Phys. Rev. Lett*. 1991, *67*, 3776-3780.

[11] Qian, Y.; d'Humi`eres, D.; Lallemand, P.; Lattice BGK Models for Navier-Stokes Equation, *Europhys. Lett*. 1992, *17*, 479-484.

[12] Fan, L. S.; Zhu, C.; Principles of Gas–Solid Flows, *Cambridge Univ. Press*, 1998.

[13] Abuzeid, S.; Busnaina, A. A.; Ahmadi, G.; Wall deposition of aerosol particles in a turbulent channel flow. *J. Aerosol Sci.* 1991, *22,* 43–62

[14] Iwan D. W.; Mason, B. A. Jr.; Equivalent linearization for systems subjected to non-stationary random excitation. *Int. J. Non-Linear Mech*. 1980*, 15*. 71–82.

[15] Orabi, I. I.; Ahmadi, G.; Nonstationary response analysis of a duffing oscillator by the Wiener–Hermite expansion method. *J. Appl. Mech*. 1987, *54* 434–440.

[16] Ramarao, B.V., Tien, C., Mohan, S.; Calculation of single fiber efficiencies for interception and impaction with superposed Brownian motion*. J. Aerosol Sci.* 1994, *25*, 295–313.

AUTHORS' ADDRESS

Huaning Zhu; Juan P Hinestroza
College of Human Ecology
242 M Van Rensselaer Hall
Cornell University
Ithaca, NY 14853
USA